

Microstructure and mechanical properties of friction stir welded ferrite-martensite DP700 steel

Mahmoudiniya, Mahdi; Kokabi, Amir Hossein; Kheirandish, Shahram; Kestens, Leo A.I.

DOI

[10.1016/j.msea.2018.09.013](https://doi.org/10.1016/j.msea.2018.09.013)

Publication date

2018

Document Version

Final published version

Published in

Materials Science and Engineering A

Citation (APA)

Mahmoudiniya, M., Kokabi, A. H., Kheirandish, S., & Kestens, L. A. I. (2018). Microstructure and mechanical properties of friction stir welded ferrite-martensite DP700 steel. *Materials Science and Engineering A*, 737, 213-222. <https://doi.org/10.1016/j.msea.2018.09.013>

Important note

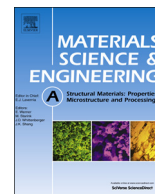
To cite this publication, please use the final published version (if applicable). Please check the document version above.

Copyright

Other than for strictly personal use, it is not permitted to download, forward or distribute the text or part of it, without the consent of the author(s) and/or copyright holder(s), unless the work is under an open content license such as Creative Commons.

Takedown policy

Please contact us and provide details if you believe this document breaches copyrights. We will remove access to the work immediately and investigate your claim.



Microstructure and mechanical properties of friction stir welded ferrite-martensite DP700 steel



Mahdi Mahmoudiniya^a, Amir Hossein Kokabi^b, Shahram Kheirandish^a, Leo A.I. Kestens^{c,d,*}

^a School of Metallurgy and Materials Engineering, Iran University of Science and Technology (IUST), Narmak, 16846-13114 Tehran, Iran

^b Department of Materials Science and Engineering, Sharif University of Technology, Azadi Ave, 145888-9694 Tehran, Iran

^c Ghent University, Metals Science and Technology Group, Technologiepark 903, B-9052 Zwijnaarde, Ghent, Belgium

^d Delft University of Technology, Department of Materials Science and Engineering, Mekelweg, 22628 CD Delft, the Netherlands

ARTICLE INFO

Keywords:

DP700 steel
Friction stir welding
Microstructure
EBSD analysis
Mechanical properties

ABSTRACT

In the present work, friction stir welding technique was applied on 2 mm thick ferrite-martensite DP700 steel sheets at rotational speeds of 600, 800 and 1000 rpm. The microstructure and mechanical properties of the welds were evaluated. It was found that Zener-Hollomon parameter decreased with increasing rotational speed that leads to grain coarsening in the stir zone. It was also found that increment of rotational speed increased softening phenomenon in sub-critical heat affected zone. The results also showed that the presence of WC particles in the stir zone, which was due to the tool wear, as well as formation of a soft ferrite band degrade the tensile properties at rotational speed of 600 rpm while HAZ softening was responsible for reduction of strength and ductility in conditions of 800 and 1000 rpm.

1. Introduction

Ferrite-martensite dual phase (DP) steels, as a type of advanced high strength steels (AHSS), are widely used for various applications, such as e.g. in the automotive industry. Actually, a good combination of strength and formability allows manufacturers to reduce the weight of vehicles while maintaining crash resistance. As the name indicates, the DP steel microstructure is composed of a hard martensite phase distributed in a soft ferrite matrix [1,2]. Welding can be considered as the main method of joining employed for DP steels, whereby the most common welding techniques include Gas Metal Arc Welding [3–5], resistance spot welding [6,7], and laser welding [8,9]. All of these methods are of the fusion welding type, in which a high amount of heat is required to locally melt the material. In the case of DP steels, this high amount of heat causes some problems such as tempering of the martensite phase leading to softening of the heat affected zone (HAZ). Formation of a softened HAZ as well as the appearance of a hard fusion zone degrade the mechanical properties of the weld [10]. These problems have persuaded researchers to investigate welding techniques with lower heat input for joining of DP steel parts. Friction stir welding (FSW) as a solid state joining technique, can be considered as a good candidate to substitute fusion welding methods. In contrast to fusion welding techniques, in FSW no melting of the materials being joined occurs during the welding. The cast microstructure of the fusion zone in

the fusion weld is replaced by a fine grained stir zone, which may show more desirable properties [11]. On the other hand, lower heat input to the weld during FSW reduces HAZ softening, which improves the formability of the welded joint. So far, only a few studies have been done on FSW of DP steels. Miles et al. [12] compared the formability of laser welded and friction stir welded DP590 steel. They observed that FSW can lead to joints that are 20% more formable than the laser welded sheets. They did not pay attention to microstructural characterization. Kim et al. [13] studied the weldability of DP590 steel, whereby the main focus of their research was on the quality of the welded joints and tool life during friction stir welding. Their results showed that the ratio of rotational speed to traveling speed has dominant effect on the joint quality. However, they did not analysis microstructure features of the weld.

Since the mechanical properties of the weld joint are controlled by the microstructure in various regions of the weld, so it is necessary to understand the microstructural changes accompanying friction stir welding. Although, limited studies [12–14] were done to evaluate the mechanical properties of the friction stir welded DP steels, there is no systematic work to evaluate the microstructural features and phase transformations in various regions of the weld, neither are there detailed literature reports on the correlation between the microstructure and resultant mechanical properties. Therefore, the present study will present part of a systematic research to explore the effect of FSW

* Corresponding author at: Ghent University, Metals Science and Technology Group, Technologiepark 903, B-9052 Zwijnaarde, Ghent, Belgium.
E-mail address: leo.kestens@ugent.be (L.A.I. Kestens).

Table 1
The chemical composition (wt%) of DP700 steel.

C	Mn	Si	S	P	Ni	Cr	Cu
0.076	1.041	0.435	0.004	0.033	0.231	0.561	0.34

Table 2
FSW parameters used for the present study.

Rotational speed (rpm)	Transverse speed (mm/min)	Tilt angle (deg.)	Tool geometry		
			Shoulder diameter (mm)	Pin diameter (mm)	Pin height (mm)
600, 800, 1000	50	3	16	6	1.8

parameters on microstructure and mechanical properties of a DP700 steel.

2. Materials and methods

The starting material in the present study was 2 mm thick DP700 steel sheet. The chemical composition of the steel is given in Table 1.

Butt weld FSW was conducted using a WC-Co tool with shoulder diameter of 16 mm, a pin diameter of 6 mm and a pin length of 1.8 mm. Using a FSW facility, welding was performed at a feed rate of 50 mm/min and with tool rotational speeds of 600, 800 and 1000 rpm. A 3° tilt was applied to the tool during welding. Table 2 summarizes the welding conditions.

The welding direction was perpendicular to the sheet rolling direction. Argon gas was used as shielding gas to protect the tool and the weld from surface oxidation. Fig. 1 shows a schematic of the welding process. Microstructural characterization was carried out by optical microscopy and field emission scanning electron microscope on weld cross-sections after polishing and etching with 3% Nital. Additionally, more detailed microstructural analysis was done with an electron backscatter diffraction (EBSD) system. For EBSD analysis, samples were electropolished with A2 electrolyte (produced by Struers[®]) at room temperature at a voltage of 36 V. The step size of 0.150 μm was used for EBSD measurements, whereby an area was scanned of 80 μm × 80 μm. Hardness measurements were made across the weld with a Vickers microhardness tester at load of 100 gr and 12 s dwell time. Tensile properties of the transverse joints were evaluated using a uniaxial tensile test facility. Transverse tensile samples were prepared by wire cutting according to ASTM-E8 [15]. The tensile tests were carried out at a cross head velocity of 1 mm/min.

3. Results and discussion

3.1. Macrostructure

The transverse macrostructures of the joints are exhibited in Fig. 2

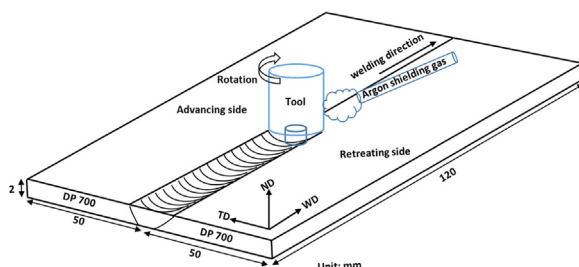


Fig. 1. A schematic presentation of friction stir butt weld for this study.



Fig. 2. Macrostructure of the cross-sections transverse to the welding direction at various rotational speeds (RS: retreating side, AS: advancing side).

and it is shown that all welds are free from crack and defects and exhibit a basin-shaped outline. It was also seen that the size of the stir zone increased with increment of rotational speed. It is well-known that the heat input and force acting per unit volume affect the stir zone size [16]. The heat input during FSW can be estimated as [17]:

$$Q = \frac{4\pi^2\mu P\omega R^3}{3V} \quad (1)$$

where Q is heat input rate per unit weld length, μ is the friction coefficient, P is pressure, ω is rotational speed, R is the shoulder radius and V is the transverse speed.

To describe the force acting per unit volume, Nandan et al. [18] developed torque-based index (TI) as:

$$TI = \frac{\omega \cdot \tau}{D_{\text{shoulder}} \cdot V \cdot A_{\text{pin}}} \quad (2)$$

where ω is rotation rate, τ is torque, D_{shoulder} is the diameter of tool shoulder, V is the transverse speed and A_{pin} is the projected area of the pin. As can be seen from Eqs. (1) and (2) both heat input and force acting per unit volume increase with increment of rotational speed. Higher heat input and force acting per unit volume caused easier material flow so the size of the stir zone increased.

3.2. Microstructure

3.2.1. Base Metal

Fig. 3 shows the microstructure of the base metal (BM), which consists of 20.7% martensite phase embedded in the ferrite matrix. In fact, the contiguous martensite network formed at the ferrite grain boundaries where the austenite phase formed at the intercritical annealing temperature.

3.2.2. Heat Affected Zone (HAZ)

The heat affected zone (HAZ) is a region adjacent to the base metal in which experiences only thermal cycle during welding. In HAZ, peak temperature increases with distance away from the base metal. Based on peak temperature, HAZ can be divided into different regions [19]: 1) Sub-critical heat affected zone (SC-HAZ), where the peak temperature is lower than Ac_1 . 2) Inter critical heat affected zone (IC-HAZ), where the peak temperature lies between Ac_1 and Ac_3 . 3) Fine grained heat affected zone (FG-HAZ), which experiences peak temperature slightly higher than Ac_3 . Each region will be described in details in the following.

3.2.2.1. Sub-critical heat affected zone (SC-HAZ). Microstructures of the sub-critical heat affected zone (SC-HAZ) are presented in Fig. 4. This region consists of ferrite and tempered martensite. Since the peak temperature in this region was below Ac_1 , any austenite phase did not form. There are some granular particles in the martensite which appear to be carbides. Actually, during tempering, the martensite phase has decomposed to carbide and recovered ferrite [20]. It can be seen that the severity of tempering increases with increment of rotational speed. The higher heat input leads to a higher residence time near peak temperature and increases tempering martensite [21].

3.2.2.2. Inter critical heat affected zone (IC-HAZ). Fig. 5 shows the microstructure of inter-critical heat affected zone (IC-HAZ) where the

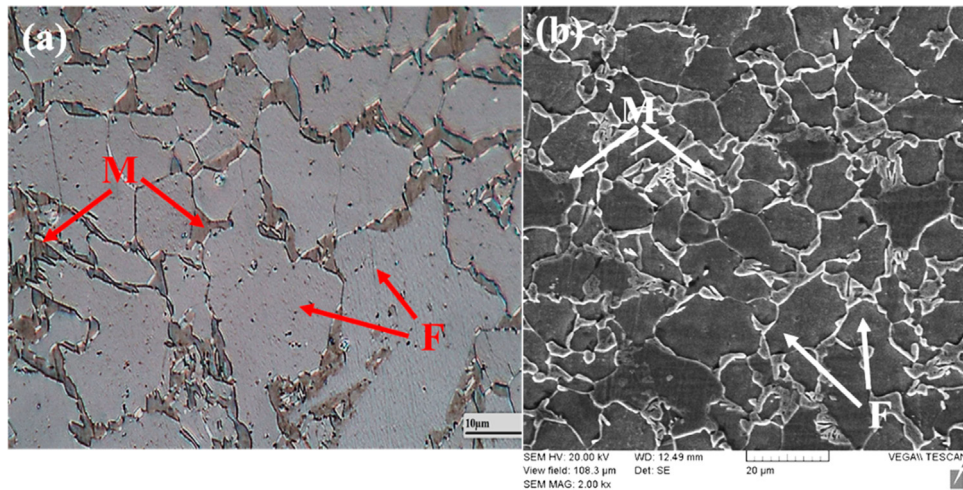


Fig. 3. Micrographs showing microstructure of base metal a) OM microstructure b) SEM microstructure (where M: martensite and F: ferrite).

material was heated to temperatures in the inter-critical domain at various rotational speeds. As can be seen, the IC-HAZ consisted of ferrite and martensite phases. In this region, the temperature has reached a value between Ac_1 and Ac_3 during the heating cycle. Accordingly, ferrite and austenite phases will form. Since the austenite coexists with ferrite, it has a larger carbon concentration than the initial steel. The higher carbon level results in higher hardenability, which leads to martensite formation during the cooling cycle.

It is also noticed that the increment of rotational speed leads to increase in volume fraction of martensite in IC-HAZ. This is due to high heat input owing to increased rotational speed.

3.2.2.3. Fine grained heat affected zone (FG-HAZ). Fig. 6 depicts the microstructure of the fine grained HAZ (FG-HAZ) of the welded samples, which consists of fine ferrite grains, martensite and bainite packets. The fine grained region is part of the supercritical HAZ that

was heated just above the Ac_3 temperature during welding, in which the primary structure has fully transformed to the austenite phase before cooling. Since the peak temperature in the FG-HAZ during the heating cycle is slightly higher than Ac_3 , the austenite grains may not be allowed to grow [22]. As can be seen, the finest structure of FG-HAZ is related to the condition of 600 rpm. It is well accepted that heat input that introduces to the weld controls the cooling rate, as well as the peak temperature in different zones of the weld, such as e.g. the heat affected zone. The heat that is introduced to the weld will dissipate through the heat affected zone. If the heat input is low, transferring or dissipation of the heat through the HAZ is faster than the condition in which a high amount of heat has introduced to the weld. Faster dissipation of heat input through the HAZ corresponds to the higher cooling rate in HAZ [22]. Accordingly, decreasing the rotational speed decreases the heat input to weld, so it can be concluded that the higher cooling rate in HAZ corresponds to the lower rotational speed. Since the higher heating rate and cooling rate corresponds to the rotational speed of 600 rpm, the

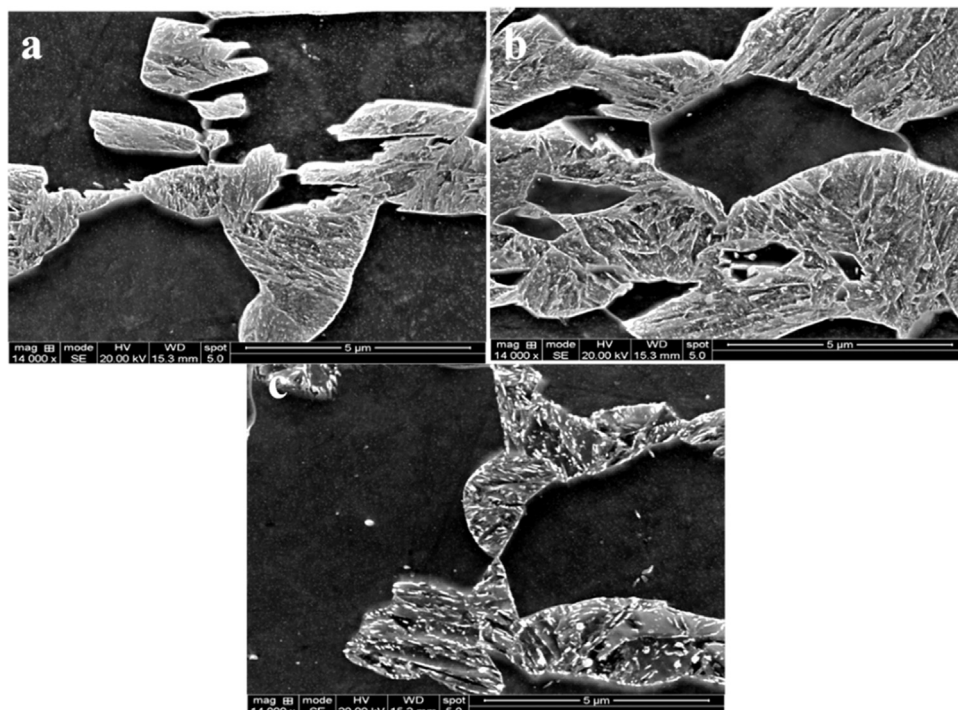


Fig. 4. SEM micrographs of sub-critical heat affected zone at rotational speed of a) 600 rpm b) 800 rpm c) 1000 rpm.

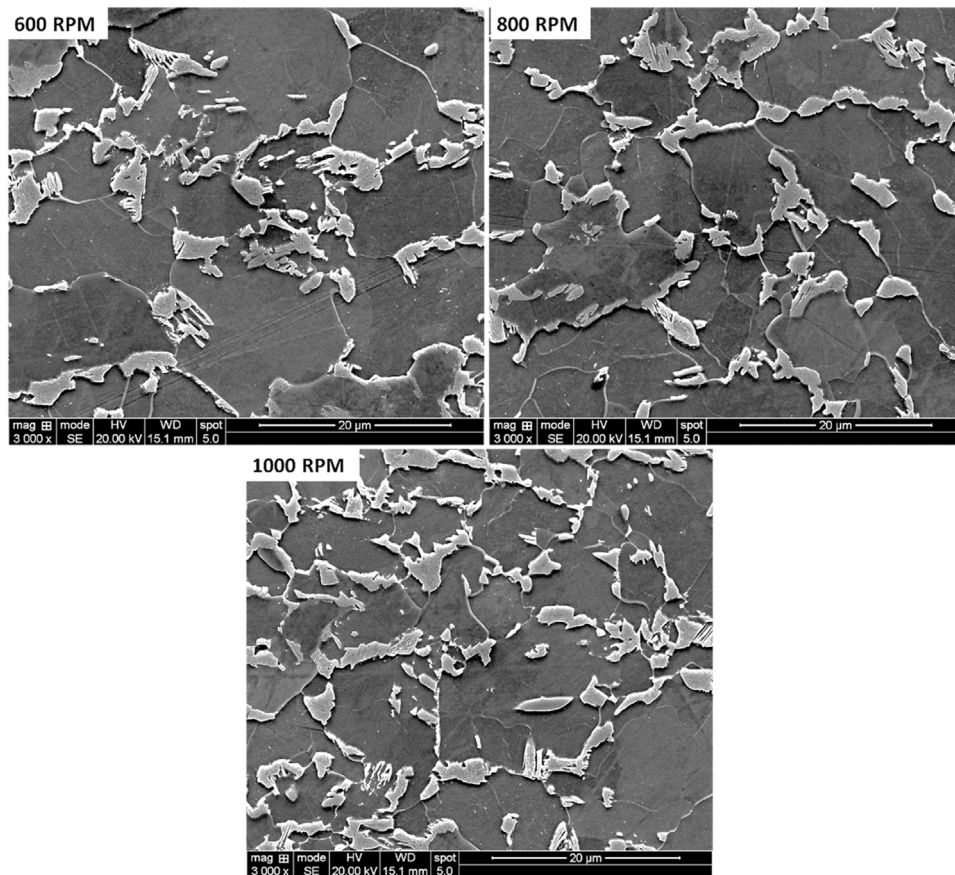


Fig. 5. SEM images for IC-HAZ at various rotational speeds.

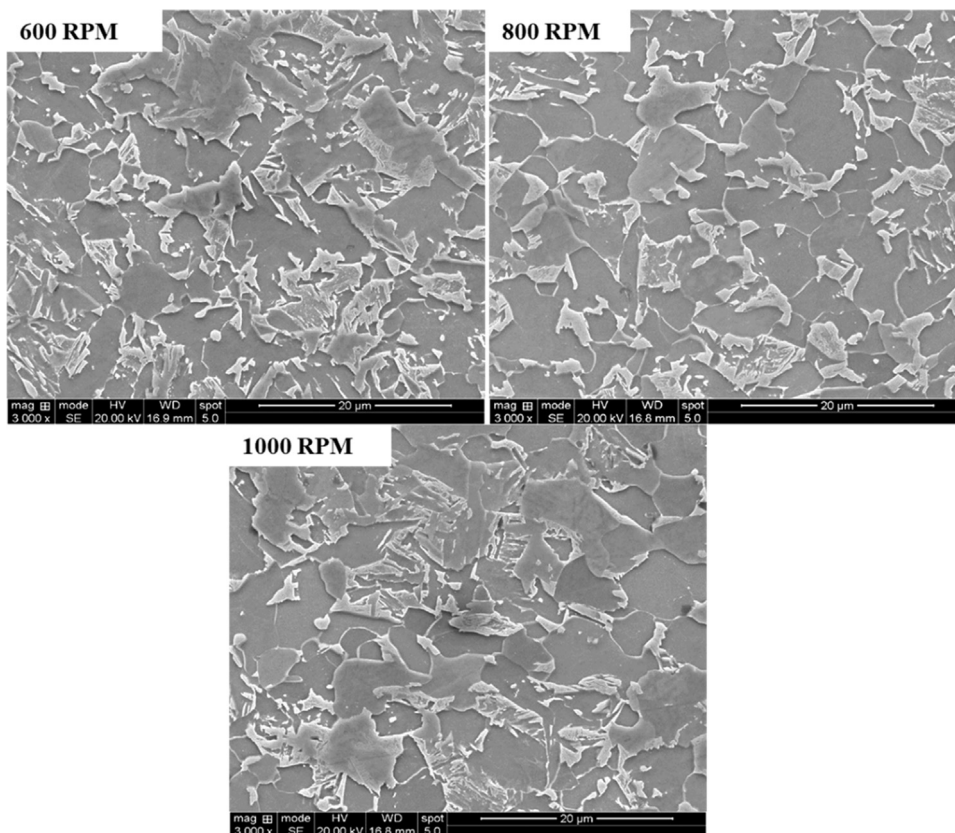


Fig. 6. Fine grained heat affected zone at different rotational speeds.

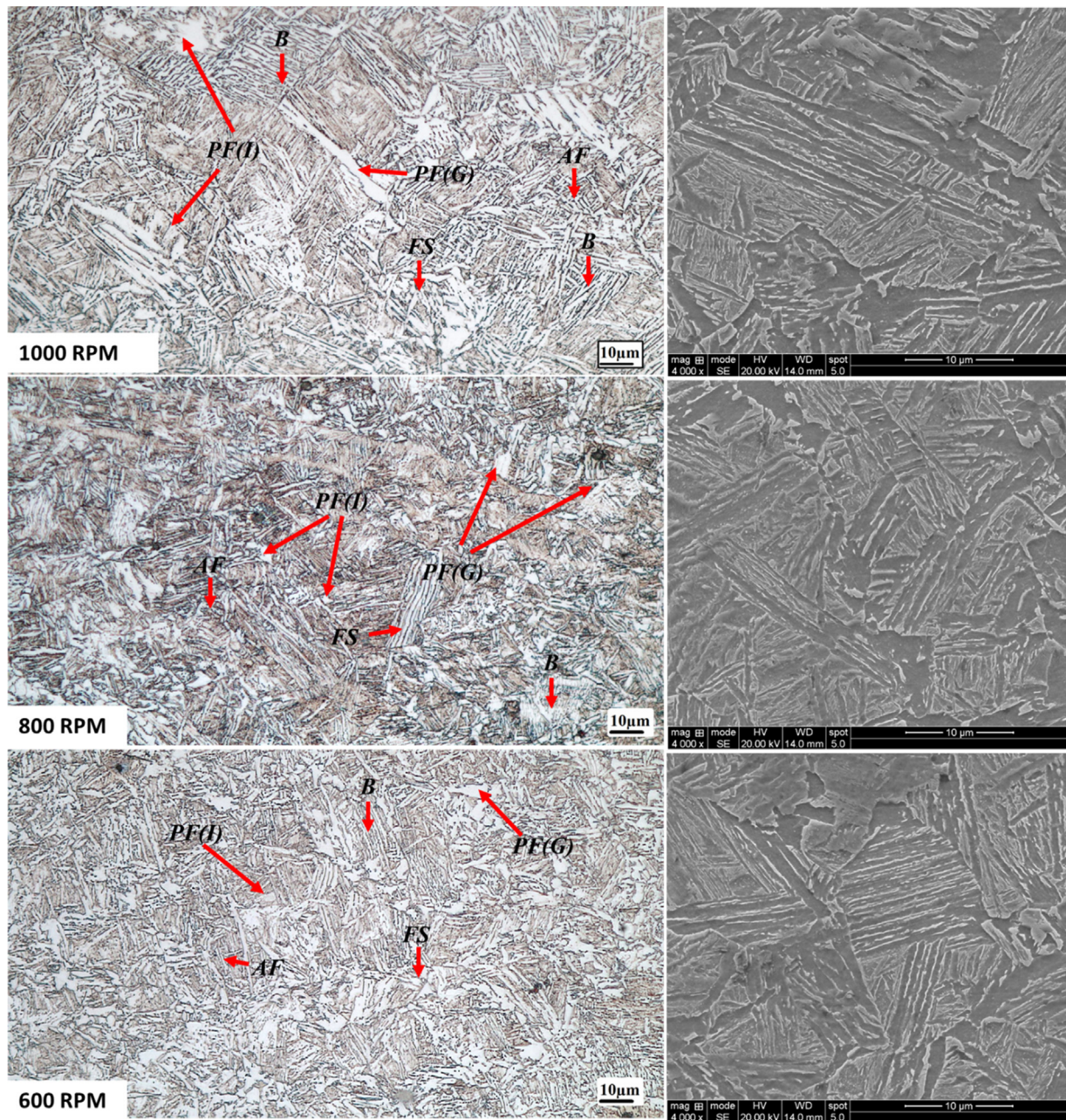


Fig. 7. Optical micrographs and FE-SEM images of SZ at various rotational speeds ((PF(G)): grain boundary ferrite, PF(I): intragranular ferrite, (FS): Widmanstätten ferrite, AF: acicular ferrite and B: bainite).

holding time above A_{c3} is minimal in this condition. It means that formed austenite grains do not have enough time for growth before cooling, which results in a finer product structure after cooling cycle.

3.2.3. Thermo-Mechanically Affected Zone (TMAZ)

It should be noted that any distinct thermo-mechanically affected zone (TMAZ) was not observed in the FSW joints in the present study. In fact, the allotropic phase transformations that take place during friction stir welding of low-carbon steels, destroy the microstructure of the TMAZ [17].

3.2.4. Stir Zone (SZ)

The microstructure of the center of SZ in various rotational speeds is shown in Fig. 7.

As can be seen, the stir zone has a complex microstructure consisting of primary ferrite (PF), widmanstätten ferrite (ferrite side plates

(FS)), acicular ferrite (AF) as well as bainite. Primary ferrite exists in two various morphologies include: grain boundary ferrite (PF(G)) and intragranular ferrite (PF(I)). The presence of primary ferrite as well as bainite shows that the peak temperature in SZ was above A_{c3} during friction stir welding. Since the SZ simultaneously experiences heat and high strain, the austenite phase recrystallizes dynamically before cooling. Fig. 8 shows the EBSD orientation maps of the stir zones observed in samples processed at different rotational speeds.

No elongated grain morphology could be observed in the stir zone processed under different conditions. It is because of the occurrence of dynamic recrystallization in the stir zone that leads to equiaxed grains before cooling cycle. Actually, it is well accepted that the stir zone undergoes dynamic recrystallization under co-presence of severe strain and high temperatures during friction stir welding [23–29]. EBSD maps are also used for the determination of the average grain size in the stir zone. Accordingly, average grain sizes of 8.6 ± 2.1 , 11.3 ± 1.9 and

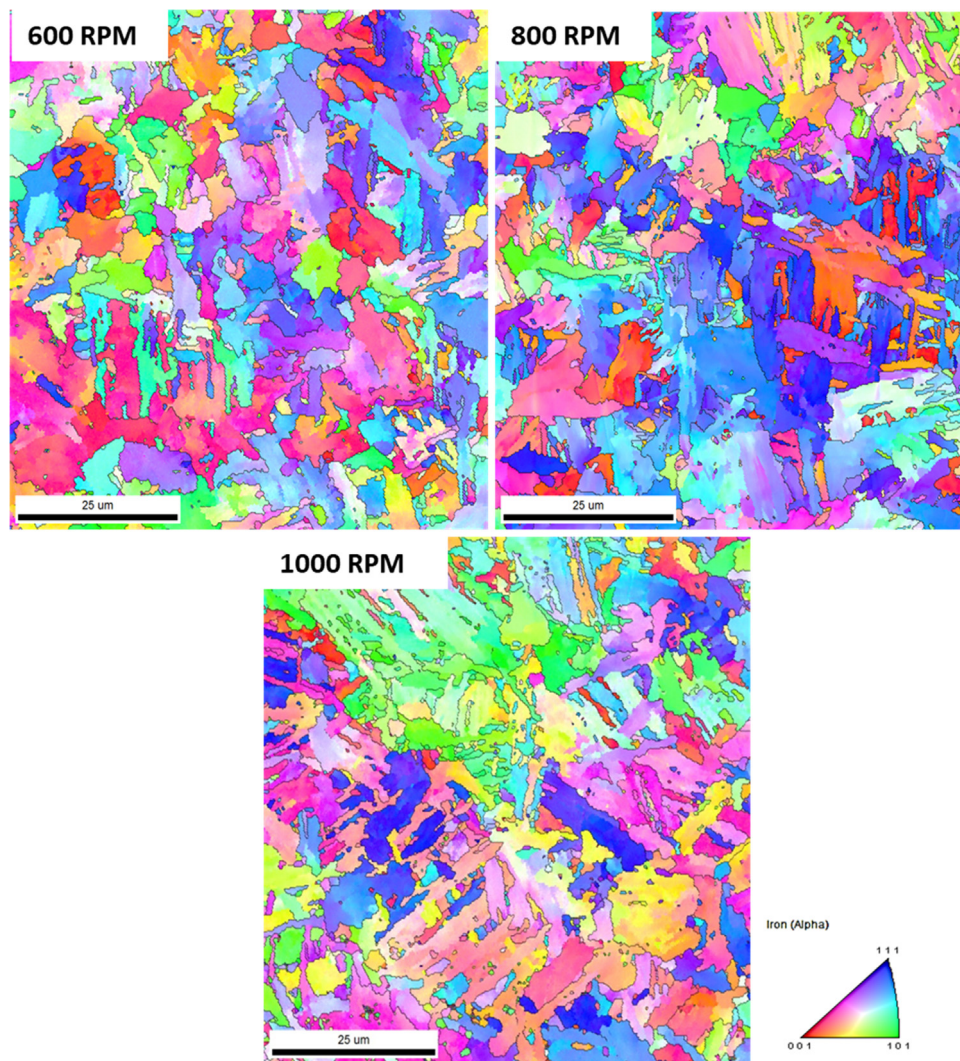


Fig. 8. EBSD orientation color maps at the center of stir zone at different rotational speeds (black lines correspond to high angle boundaries ($\geq 15^\circ$)).

$13.9 \pm 2 \mu\text{m}$ were obtained with rotational speeds of 600, 800 and 1000 rpm, respectively. It also should be noted that the reported values are an average of various different EBSD maps and the misorientation angle of 15° was used for grain boundary definition. These results indicate to structural coarsening with increasing rotational speed. Some points are worth noting on grain size determination via EBSD measurements. Since all of the existing phases in the stir zone originated from recrystallized austenite phase, the prior austenite grain size largely affects the average grain size of the stir zone [30]. It should be noted that the formation of grain boundary ferrite deletes some primary austenite grain boundaries, which makes it more challenging to determine quantitatively the prior austenite grain size (PAGS). However, by considering FSW as a thermomechanical process, the Zener-Hollomon parameter (Z parameter) can be utilized for determination of the grain size of the recrystallized austenite, qualitatively. The dynamically recrystallized grain size (D) has an inverse relation with the Z parameter as [31]:

$$D = \frac{1}{a + b \ln(Z)} \quad (3)$$

where a and b are material constants. The Z parameter can be written as [32]:

$$Z = \dot{\epsilon} \exp\left(\frac{Q}{RT}\right) \quad (4)$$

where $\dot{\epsilon}$ is the strain rate, R is the gas constant, Q is the activation energy for the deformation process and T is the process temperature. A literature reported [33] value of 280 kJ/mol was used for the activation energy for deformation. Chang et al. [34] simulated the friction stir processing. They considered that all material in the stir zone (or dynamically recrystallized region) experience a plastic flow. By assuming a torsion type deformation, they calculated the strain rate as:

$$\dot{\epsilon} = \frac{R_m 2\pi r_e}{L_e} \quad (5)$$

R_m is average material flow rate which, by a linear assumption, can be considered about half of the rotational speed. L_e refers to the effective depth of the dynamically recrystallized zone which is about $\pi/4$ of shoulder radius, and r_e is the effective radius of the dynamically recrystallized zone, about $\pi/4$ of the plunge depth [34]. T is the peak temperature (T_p) of the SZ, which can be approximated by the following expression [35]:

$$\frac{T_p}{T_m} = K \left(\frac{\omega^2}{V \times 10^4} \right)^\alpha \quad (6)$$

where T_m is melting point of material, V is the traversing speed, ω is rotational speed, K and α are constants, which can be estimated as 0.05 and 0.7 [16,35,36], respectively.

The calculation results for strain rate, peak temperature and Z parameter are summarized in Table 3.

Table 3

Calculated values of peak temperature, strain rate and Zener-Hollomon parameter at various tool rotational speeds.

Rotational speed (rpm)	Peak temperature (K)	Strain rate (1/S)	Z parameter ($\times 10^{13}$)
600	1257	139	5.93
800	1286	186	4.35
1000	1309	232	3.44

It can be seen that strain rate increases from 139 to 232 s⁻¹ with increasing rotational speed from 600 to 1000 rpm. In general, the increase of strain rate, without considering other parameters, increases the Z parameter, which produces a finer recrystallized grain size. But the role of temperature also should be taken into account. Increasing the rotational speed from 600 to 1000 rpm increases the temperature from 1257 to 1309 K. The rise of temperature decreases the Z parameter, producing an increase of the recrystallized grain size. The present data show that the temperature has the dominant effect on the grain size of dynamically recrystallized austenite.

Since the Z parameter experienced a decreasing trend with increasing rotational speed, hence the coarsening of the microstructure with increasing rotational speed can be explained by considering the Zener-Hollomon parameter.

Fig. 7 also shows that grain boundary ferrite, produced at 1000 rpm, is coarser than observed with 600 or 800 rpm rotation speed. The primary austenite grain size in the SZ is highest at the largest rotational speed because the lowest Z parameter is associated with the largest rotational speed, hence less grain boundaries are available as nucleation sites for primary ferrite, leading to a smaller number of ferrite nuclei from the primary austenite grain boundaries. Additionally, the cooling rate is lowest at higher rotation speeds, thus ferrite nucleus have more time to grow. Fig. 7 also revealed that a higher amount of acicular ferrite has formed at lower rotational speed condition. As discussed above, the lower rotational speed decreases the heat input to the weld and leads to higher cooling rates, which gives rise to the preferential formation of acicular ferrite as compared to polygonal ferrite [37]. Additionally, the formation of grain boundary ferrite at the prior austenite grain boundaries affects the formation of acicular ferrite. Lee et al. [38] reported that formation of acicular ferrite is promoted by the formation of grain boundary ferrite. Actually, decorating austenite grain boundaries with fine allotriomorphic ferrite renders the boundaries inert to the formation of bainite sheaves.

A noticeable point is that a narrow band of ferrite can be seen at the lower part of the stir zone formed with a rotational speed of 600 rpm, cf. Fig. 9. This band has elongated into the stir zone. The appearance of this ferrite band is also reported during FSW or FSSW of steels by other researchers [36,39–42]. The formation mechanism of this ferritic layer is not yet fully understood. Hovanski et al. [42] reported that the ferrite phase can be stabilized via decarburization of surface during processing and the formed ferrite pulled through the weld

It also observed that there are some particles in the stir zone of the



Fig. 9. Formation of a band of ferrite in SZ at tool rotational speed of 600 rpm.

600 rpm weld (Fig. 10.a), whereby the EDS results (Fig. 10.b) showed that they are WC particles. In fact, the presence of WC particles in the stir zone indicates the wear of the tool material during friction stir welding, whereby the worn tool material was inserted in the weld. It is notable that the issue of tool wear during friction stir welding of steels has been reported by other researchers [43–45].

3.3. Mechanical properties

3.3.1. Hardness measurement

Fig. 11 shows the microhardness profiles across the welds. The average hardness of the base material was 275 ± 3 HV.

In all samples, by moving from BM toward the center line of the stir zone, the microhardness experienced a decreasing trend that corresponds to SC-HAZ. The lowest hardness of the weld was located at the boundary between SC-HAZ and IC-HAZ. Actually, softening phenomenon decreases the hardness in SC-HAZ. Tempering of martensite as well as a decreasing dislocations density in original ferrite can be considered as two mechanisms for softening in SC-HAZ [46]. The highest hardness reduction corresponded to the rotational speed of 1000 rpm. Since the maximum softening is proportional to highest heat input, so the highest reduction of hardness is related to rotational speed of 1000 rpm. By entering the IC-HAZ the microhardness increases because of the formation of additional martensite after partial austenization and subsequent cooling cycle (Fig. 5). The higher hardness corresponds to the stir zone for all rotational speeds. This is attributed to grain refinement as well as the formation of hard phases such as martensite, bainite and acicular ferrite during cooling. It can also be seen that the higher hardness of the stir zone is related to the FSW condition at a rotational speed of 600 rpm. It is because of finest microstructure (highest Zener-Hollomon parameter) and the higher cooling rate in the SZ corresponding to this condition.

At the tool rotation speed of 600 rpm, in spite of the higher mean hardness, a sudden drop in microhardness at the center of the stir zone can be seen, which is caused by the presence of ferrite band in the SZ, cf. Fig. 9.

3.3.2. Tensile properties

Fig. 12 shows the engineering stress–engineering strain curves of BM and welded samples. Failure locations of welded samples are also shown in this figure. As can be seen, in the condition of 600 rpm, the failure occurred at SZ while in rotational speeds of 800 and 1000 rpm, the failure takes place in the SC-HAZ.

The curve related to BM shows continuous yielding, without yield phenomenon, while the welded samples exhibit a distinct yielding point elongation. The reappearance of the yield point phenomenon in FSWed samples might be due to diffusion of interstitial atoms to the dislocations at the ferrite phase in the SC-HAZ during welding, henceforth pinning the dislocations and producing a yield point phenomenon [47]. The results of the tensile test are summarized in Table 4.

It can be seen that the welded samples showed higher yield strength than BM, which also has been reported by some other researchers [48]. The temperature generated during the welding process causes to diffusion of the solute atoms (especially interstitial atoms such as carbon) to dislocations as high energy positions whereby the dislocations are anchored in position by an atmosphere of the solute atoms. Because of the strong interaction between the solute atoms and dislocations the higher stress is required to tear away a pinned dislocation from its atmosphere, whereby the yield strength of the welded sample increases. When the pinned dislocations break away from their atmosphere they could slip at a lower stress which results to exhibition of the yield point phenomena [48–50]. While the yield strength of welded samples was higher than the base metal, all welded samples showed lower ultimate strength and elongation than BM. The minimum of ultimate strength is related to sample with rotational speed of 600 rpm (about 87.5% of BM). Moreover, the 600 rpm weld exhibited the lowest elongation

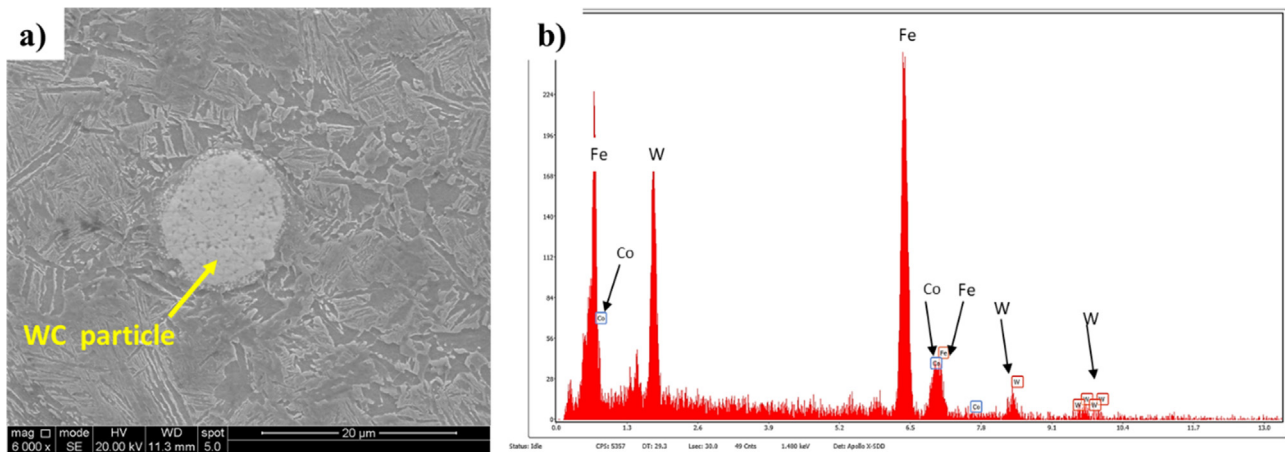


Fig. 10. a) Presence of some particles in the stir zone of the 600 rpm weld b) The result of the EDS analysis of the particles.

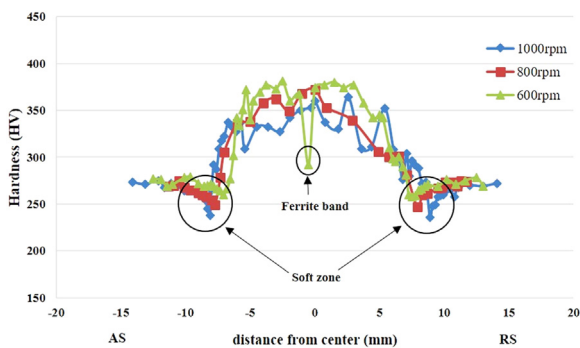


Fig. 11. Microhardness distribution for joints on the center line.

Table 4

Tensile test results with different rotational speeds.

Tool rotational speed (rpm)	Yield strength (MPa)	Ultimate tensile strength (MPa)	Total elongation (%)	Failure location	Joint efficiency (%)
Base Metal	474 ± 3	723 ± 5	20.1 ± 1	–	–
600	487 ± 4	633 ± 3	4.7 ± 0.7	SZ	87.5
800	481 ± 2	662 ± 1	10.7 ± 0.5	HAZ	91.5
1000	479 ± 2	644 ± 3	9.2 ± 0.4	HAZ	89

results showed that they consist of WC particles. In fact, the presence of these particles provides suitable conditions for crack nucleation, whereby strength and ductility decrease.

Moreover, the formation of a soft ferrite band in SZ can also contribute to degradation of the mechanical properties of the 600 rpm weld, as the presence of this band provides suitable conditions for crack propagation through this soft region and therefore decreases both the tensile strength and ductility [36,39].

By increment of rotational speed to 800 rpm the ultimate strength and ductility increase to 662 MPa and 10.7%, respectively, but it is still lower than those of the base metal. The change in mechanical properties compared to the 600 rpm weld is induced by the absence of WC particles as well as the disappearance of the ferrite band. During tensile test of the 800 and 1000 rpm welded samples, the softest zone is the stir zone, which yields first and accommodates the majority of subsequent plastic deformation, leading to an earlier necking and premature fracture. Accordingly, the overall elongation of the welded sample will decrease compared to the base metal.

By increasing rotational speed to 1000 rpm, the ultimate strength and elongation experience a decreasing trend again. In this case the failure location remains at SC-HAZ. Increment of rotational speed leads to more intense softening at SC-HAZ, as explained before. So decreasing strength and ductility in condition of 1000 rpm is reasonable.

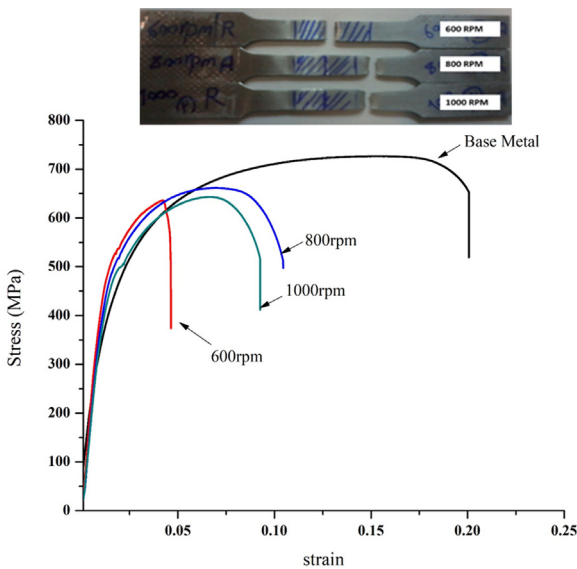


Fig. 12. Engineering stress-Engineering strain curves of base metal and welded samples.

compared to the other welds (total elongation of 4.7%). As mentioned, the weld applied with 600 rpm rotational speed has failed in the stir zone which clearly shows that the softening phenomenon in the SC-HAZ is not responsible for the fracture. Researchers have reported that the presence of worn tool particles in the stir zone can degrade the tensile properties of the joint [43]. To evaluate this, the fracture surface of the welds were examined by SEM, cf. Fig. 13. As can be seen, the fracture surface of the 600 rpm weld contains some particles of which the EDS

4. Conclusions

In the present work, friction stir welding of DP700 steel was done at various rotational speeds. Detailed evaluation of microstructure and mechanical properties in a friction stir welded DP700 steel was carried out. The major findings can be summarized as follows:

- 1) In all various rotational rates the stir zone experiences a temperature higher than Ac₃ critical temperature, and formed austenite was transformed to different products during cooling cycle. Prior austenite grain size will reduce by decreasing of rotational speed that

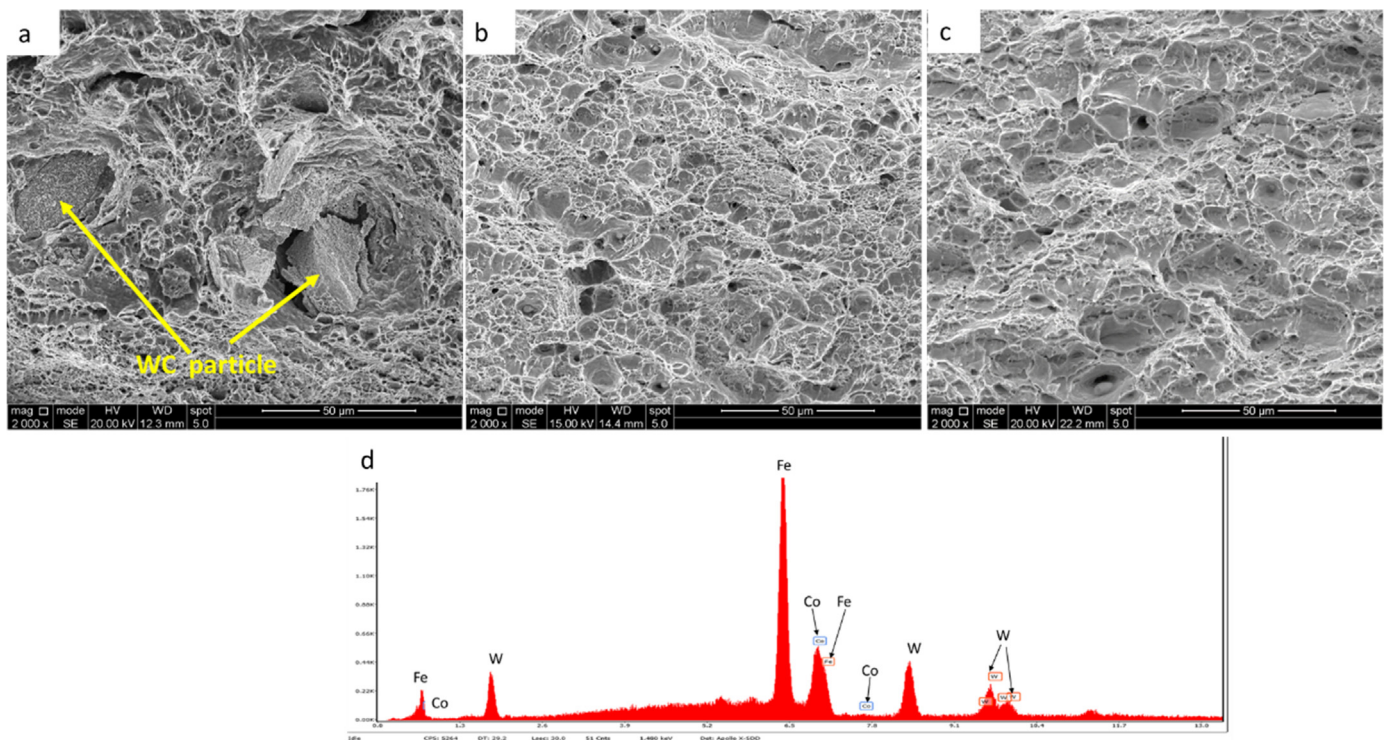


Fig. 13. a) Fracture surface of the welded joints at rotational speed of a) 600 rpm, b) 800 rpm c) 1000 rpm and d) EDS result for the particles in Fig. 13a.

leads to a finer microstructure after cooling. Additionally, higher cooling rates experience at lower rotational rate. The highest hardness in stir zone is related to lowest rotational speed.

- Sub-critical HAZ experiences higher peak temperature (but below A_{c1}) and lower cooling rates at higher rotational speeds. BM is exposed to higher temperatures for longer times under higher rotational speeds conditions, and leads to a higher degree of softening, so the minimum hardness in sub-critical HAZ is related to the condition of 1000 rpm.
- Under condition of 600 rpm a soft ferrite band forms in stir zone. Tool wear as well as formation of this ferrite layer result to occurrence of failure at the stir zone which leads to reduction of strength and ductility. In conditions of rotational speeds of 800 and 1000 rpm joints failed at softened HAZ. Higher joint strength and ductility was related to rotational speed of 800 rpm.

References

- R. Kuziak, R. Kawalla, S. Waegler, Advanced high strength steels for automotive industry, *Arch. Civ. Mech. Eng.* 8 (2008) 103–117, [https://doi.org/10.1016/S1644-9665\(12\)60197-6](https://doi.org/10.1016/S1644-9665(12)60197-6).
- H. Aydin, E. Essadiqi, I.-H. Jung, S. Yue, Development of 3rd generation AHSS with medium Mn content alloying compositions, *Mater. Sci. Eng. A* 564 (2013) 501–508, <https://doi.org/10.1016/j.msea.2012.11.113>.
- K. Mukherjee, A. Ramazani, L. Yang, U. Prah, W. Bleck, U. Reisgen, M. Schleser, A. Abdurakhmanov, Characterization of gas metal arc welded hot rolled DP600 steel, *Steel Res. Int.* 82 (2011) 1408–1416, <https://doi.org/10.1002/srin.201100152>.
- A. Ramazani, Y. Li, K. Mukherjee, U. Prah, W. Bleck, A. Abdurakhmanov, M. Schleser, U. Reisgen, Microstructure evolution simulation in hot rolled DP600 steel during gas metal arc welding, *Comput. Mater. Sci.* 68 (2013) 107–116, <https://doi.org/10.1016/j.commatsci.2012.09.009>.
- H. Ashrafi, M. Shamanian, R. Emadi, N. Saeidi, Microstructure, Tensile properties and work hardening behavior of GTA-welded Dual-phase steels, *J. Mater. Eng. Perform.* 26 (2017) 1414–1423, <https://doi.org/10.1007/s11665-017-2544-7>.
- Y.B. Li, D.L. Li, S.A. David, Y.C. Lim, Z. Feng, Microstructures of magnetically assisted dual-phase steel resistance spot welds, *Sci. Technol. Weld. Join.* 21 (2016) 555–563, <https://doi.org/10.1080/13621718.2016.1141493>.
- M. Pouranvari, S.P.H. Marashi, D.S. Safanama, Failure mode transition in AHSS resistance spot welds. Part II: Experimental investigation and model validation, *Mater. Sci. Eng. A* 528 (2011) 8344–8352, <https://doi.org/10.1016/j.msea.2011.08.01610.1016>.
- J. Wang, L. Yang, M. Sun, T. Liu, H. Li, Effect of energy input on the microstructure and properties of butt joints in DP1000 steel laser welding, *Mater. Des.* 90 (2016) 642–649, <https://doi.org/10.1016/j.matdes.2015.11.006>.
- A. Salminen, F. Farrokhi, A. Unt, I. Poutiainen, Effect of optical parameters on fiber laser welding of ultrahigh strength steels and weld mechanical properties at subzero temperatures, *J. Laser Appl.* 28 (2016), <https://doi.org/10.2351/1.4943914>.
- M. Shome, M. Tumuluru, Welding and Joining of Advanced High Strength Steels (AHSS), (2015), <https://doi.org/10.1016/C2013-0-16259-9>.
- R.S. Mishra, P.S. De, N. Kumar, Friction Stir Welding and Processing: Science and Engineering, (2014), <https://doi.org/10.1007/978-3-319-07043-8>.
- M.P. Miles, J. Pew, T.W. Nelson, M. Li, Comparison of formability of friction stir welded and laser welded dual phase 590 steel sheets, *Sci. Technol. Weld. Join.* 11 (2006) 384–388, <https://doi.org/10.1179/174329306X107737>.
- Y.G. Kim, J.S. Kim, I.J. Kim, Effect of process parameters on optimum welding condition of DP590 steel by friction stir welding, *J. Mech. Sci. Technol.* 28 (2014) 5143–5148, <https://doi.org/10.1007/s12206-014-1138-7>.
- M. Matsushita, Y. Kitani, R. Ikeda, M. Ono, H. Fujii, Y.-D. Chung, Development of friction stir welding of high strength steel sheet, *Sci. Technol. Weld. Join.* 16 (2011) 181–187, <https://doi.org/10.1179/1362171810Y.0000000026>.
- ASTM Standard E 8, Standard Test Methods for Tension Testing of Metallic Materials, 03.01, ASTM, 2000.
- M.M. Husain, R. Sarkar, T.K. Pal, N. Prabhu, M. Ghosh, Friction stir welding of steel: heat input, microstructure, and mechanical property co-relation, *J. Mater. Eng. Perform.* 24 (2015) 3673–3683, <https://doi.org/10.1007/s11665-015-1652-5>.
- Ø. Frigaard, Ø. Grong, O.T. Midling, A process model for friction stir welding of age hardening aluminum alloys, *Metall. Mater. Trans. A* 32 (2001) 1189–1200, <https://doi.org/10.1007/s11661-001-0128-4>.
- R. Nandan, G.G. Roy, T.J. Lienert, T. Debroy, Numerical modelling of 3D plastic flow and heat transfer during friction stir welding of stainless steel, *Sci. Technol. Weld. Join.* 11 (2006) 526–537, <https://doi.org/10.1179/174329306X107692>.
- H.K.D.H. Bhadeshia, R. Honeycombe, Steels: Microstructure and Properties, (2011) <http://www.sciencedirect.com/science/book/9780857094360>.
- J. Wang, L. Yang, M. Sun, T. Liu, H. Li, A study of the softening mechanisms of laser-welded DP1000 steel butt joints, *Mater. Des.* 97 (2016) 118–125, <https://doi.org/10.1016/j.matdes.2016.02.071>.
- E. Biro, J.R. McDermid, J.D. Embury, Y. Zhou, Softening kinetics in the subcritical heat-affected zone of dual-phase steel welds, *Metall. Mater. Trans. A Phys. Metall. Mater. Sci.* 41 (2010) 2348–2356, <https://doi.org/10.1007/s11661-010-0323-2>.
- S. Kou, *Welding Metallurgy*, 2nd ed., (2003).
- M.H. Razmpoosh, A. Zarei-Hanzaki, S. Heshmati-Manesh, S.M. Fatemi-Varzaneh, A. Marandi, The grain structure and phase transformations of TWIP steel during friction stir processing, *J. Mater. Eng. Perform.* 24 (2015) 2826–2835, <https://doi.org/10.1007/s11665-015-1557-3>.
- T.J. Lienert, W.L. Stellwag Jr, B.B. Grimmer, R.W. Warke, Friction stir welding studies on mild steel, *Weld. J.* 82 (2003) 1/s–9/s <https://www.scopus.com/inward/record.uri?eid=2-s2.0-0037277560&partnerID=40&md5=12d373af9902efeb20b7df73beb3513c>.
- R. Ueki, H. Fujii, L. Cui, A. Nishioka, K. Kunishige, K. Nogi, Friction stir welding of

- ultrafine grained plain low-carbon steel formed by the martensite process, *Mater. Sci. Eng. A* 423 (2006) 324–330, <https://doi.org/10.1016/j.msea.2006.02.038>.
- [26] F.H.C.H. Young Dong, N. Kazuhiro, N. Kiyoshi, Friction stir welding of high carbon tool steel (SK85) below eutectoid temperature, *Trans. JWRI* 38 (2009).
- [27] M.H. Razmpoosh, A. Zarei-Hanzaki, A. Imandoust, Effect of the Zener-Hollomon parameter on the microstructure evolution of dual phase TWIP steel subjected to friction stir processing, *Mater. Sci. Eng. A* 638 (2015) 15–19, <https://doi.org/10.1016/j.msea.2015.04.022>.
- [28] H.H. Cho, D.W. Kim, S.T. Hong, Y.H. Jeong, K. Lee, Y.G. Cho, S.H. Kang, H.N. Han, Three-dimensional numerical model considering phase transformation in friction stir welding of steel, *Metall. Mater. Trans. A Phys. Metall. Mater. Sci.* 46 (2015) 6040–6051, <https://doi.org/10.1007/s11661-015-3177-9>.
- [29] S. Ragu Nathan, V. Balasubramanian, S. Malarvizhi, A.G. Rao, Effect of tool shoulder diameter on stir zone characteristics of friction stir welded HSLA steel joints, *Trans. Indian Inst. Met.* 69 (2016) 1861–1869, <https://doi.org/10.1007/s12666-016-0846-3>.
- [30] M. Imam, R. Ueji, H. Fujii, Microstructural control and mechanical properties in friction stir welding of medium carbon low alloy S45C steel, *Mater. Sci. Eng. A* 636 (2015) 24–34, <https://doi.org/10.1016/j.msea.2015.03.089>.
- [31] A. Rollett, F.J. Humphreys, G.S. Rohrer, M. Hatherly, *Recrystallization and Related Annealing Phenomena*, Elsevier, 2004.
- [32] K. Huang, R.E.E. Logé, A review of dynamic recrystallization phenomena in metallic materials, *Mater. Des.* 111 (2016) 548–574, <https://doi.org/10.1016/j.matdes.2016.09.012>.
- [33] P. Suwanpinij, U. Prael, W. Bleck, R. Kawalla, Fast algorithms for phase transformations in dual phase steels on a hot strip mill run-out table (ROT), *Arch. Civ. Mech. Eng.* 12 (2012) 305–311, <https://doi.org/10.1016/j.acme.2012.06.004>.
- [34] C.I. Chang, C.J. Lee, J.C. Huang, Relationship between grain size and Zener-Hollomon parameter during friction stir processing in AZ31 Mg alloys, *Scr. Mater.* 51 (2004) 509–514, <https://doi.org/10.1016/j.scriptamat.2004.05.043>.
- [35] M. Ghosh, K. Kumar, R.S. Mishra, Analysis of microstructural evolution during friction stir welding of ultrahigh-strength steel, *Scr. Mater.* 63 (2010) 851–854, <https://doi.org/10.1016/j.scriptamat.2010.06.032>.
- [36] M. Ghosh, K. Kumar, R.S. Mishra, Friction stir lap welded advanced high strength steels: microstructure and mechanical properties, *Mater. Sci. Eng. A* 528 (2011) 8111–8119, <https://doi.org/10.1016/j.msea.2011.06.087>.
- [37] R. Ghomashchi, W. Costin, R. Kurji, Evolution of weld metal microstructure in shielded metal arc welding of X70 HSLA steel with cellulosic electrodes: a case study, *Mater. Character.* 107 (2015) 317–326, <https://doi.org/10.1016/j.matchar.2015.07.032>.
- [38] C.H. Lee, H.K.D.H. Bhadeshia, H.-C.C. Lee, Effect of plastic deformation on the formation of acicular ferrite, *Mater. Sci. Eng. A* 360 (2003) 249–257, [https://doi.org/10.1016/S0921-5093\(03\)00477-5](https://doi.org/10.1016/S0921-5093(03)00477-5).
- [39] R. Sarkar, T.K. Pal, M. Shome, Microstructures and properties of friction stir spot welded DP590 dual phase steel sheets, *Sci. Technol. Weld. Join.* 19 (2014) 436–442, <https://doi.org/10.1179/1362171814Y.0000000210>.
- [40] K. Aota, K. Ikeuchi, Development of friction stir spot welding using rotating tool without probe and its application to low carbon steel plates, *Yosetsu Gakkai Ronbunshu/Q. J. Jpn. Weld. Soc.* 26 (2008) 54–60, <https://doi.org/10.2207/qjwjs.26.54>.
- [41] M. Ghosh, K. Kumar, R.S. Mishra, Process optimization for friction-stir-welded martensitic steel, *Metall. Mater. Trans. A Phys. Metall. Mater. Sci.* 43 (2012) 1966–1975, <https://doi.org/10.1007/s11661-012-1084-x>.
- [42] Y. Hovanski, M.L. Santella, G.J. Grant, Friction stir spot welding of hot-stamped boron steel, *Scr. Mater.* 57 (2007) 873–876, <https://doi.org/10.1016/j.scriptamat.2007.06.060>.
- [43] M. Jafarzadegan, A.H. Feng, A. Abdollah-Zadeh, T. Saeid, J. Shen, H. Assadi, Microstructural characterization in dissimilar friction stir welding between 304 stainless steel and st37 steel, *Mater. Character.* 74 (2012) 28–41, <https://doi.org/10.1016/j.matchar.2012.09.004>.
- [44] S.J. Barnes, A.R. Bhatti, A. Steuwer, R. Johnson, J. Altenkirch, P.J. Withers, Friction stir welding in HSLA-65 steel: Part I. Influence of weld speed and tool material on microstructural development, *Metall. Mater. Trans. A Phys. Metall. Mater. Sci.* 43 (2012) 2342–2355, <https://doi.org/10.1007/s11661-012-1110-z>.
- [45] A. Steuwer, S.J. Barnes, J. Altenkirch, R. Johnson, P.J. Withers, Friction stir welding of HSLA-65 steel: Part II. The influence of weld speed and tool material on the residual stress distribution and tool wear, *Metall. Mater. Trans. A Phys. Metall. Mater. Sci.* 43 (2011) 2356–2365, <https://doi.org/10.1007/s11661-011-0643-x>.
- [46] J. Wang, L. Yang, M. Sun, T. Liu, H. Li, A study of the softening mechanisms of laser-welded DP1000 steel butt joints, *Mater. Des.* 97 (2016) 118–125, <https://doi.org/10.1016/j.matdes.2016.02.071>.
- [47] N. Farabi, D.L. Chen, Y. Zhou, Microstructure and mechanical properties of laser welded dissimilar DP600/DP980 dual-phase steel joints, *J. Alloy. Compd.* 509 (2011) 982–989, <https://doi.org/10.1016/j.jallcom.2010.08.158>.
- [48] N. Farabi, D.L. Chen, Y. Zhou, Tensile properties and work hardening behavior of laser-welded dual-phase steel joints, *J. Mater. Eng. Perform.* 21 (2012) 222–230, <https://doi.org/10.1007/s11665-011-9865-8>.
- [49] G. Dieter, *Mechanical Metallurgy*, McGraw-hill, New York, 1986, [https://doi.org/10.1016/S0016-0032\(62\)91145-6](https://doi.org/10.1016/S0016-0032(62)91145-6).
- [50] N. Farabi, D.L. Chen, J. Li, Y. Zhou, S.J. Dong, Microstructure and mechanical properties of laser welded DP600 steel joints, *Mater. Sci. Eng. A* 527 (2010) 1215–1222, <https://doi.org/10.1016/j.msea.2009.09.051>.